# A MONTE CARLO ANALYSIS OF CONTINGENCY OPTIMAL GUIDANCE FOR MARS ENTRY

# Emily M. Palmer\* and Anil V. Rao†

A Monte Carlo analysis of a contingency optimal guidance strategy is conducted. The guidance strategy is applied to a Mars Entry problem in which it is assumed that the surface level atmospheric density is a random variable. First, a nominal guidance strategy is employed such that the optimal control problem is re-solved at constant guidance cycles. When the trajectory lies within a particular distance from a path constraint boundary, the nominal guidance strategy is replaced with a contingency guidance strategy, where the contingency guidance strategy attempts to prevent a violation in the the relevant path constraint. The contingency guidance strategy utilizes the reference optimal control problem formulation, but modifies the objective functional to maximize the margin between the path constraint limit and path constraint function value. The ability of the contingency guidance strategy to prevent violations in the path constraints is assessed via a Monte Carlo simulation.

#### INTRODUCTION

Performance optimization in Mars entry, descent, and landing is a challenging problem. One aspect that adds such complexity is the path constraints that must be imposed on the vehicle during entry, that is, constraints must be placed on key quantities such as the dynamic pressure, the acceleration load, and the heating rate. Typically the optimal control problem is solved offline in the mission planning phase. During flight, however, it is likely that the vehicle will deviate from the reference solution (which was computed offline) due to modeling errors and disturbances. As a result of such deviations from the reference in the actual flight, it is necessary to perform guidance corrections during entry. These guidance command corrections must not only ensure the vehicle stays within desired limits of the objective, but must also ensure the vehicle does not violate key constraints. This paper considers a guidance strategy that re-solves the optimal control problem at constant guidance cycles while simultaneously allowing for a contingency mode that prevents path constraints from being violated. The effectiveness of this contingency guidance strategy is evaluated in this paper via Monte Carlo simulation.

It is known that once a vehicle is perturbed off its nominal trajectory, the quality of the solution can quickly degrade. Moreover, if the deviation from the nominal is sufficiently large, it is possible that the optimal control problem may not have a feasible solution. Different approaches have been considered to reduce the effect of disturbances and uncertainties during the actual motion of the vehicle. On of these approaches is called desensitized optimal control (DOC). DOC was first proposed

<sup>\*</sup>Ph.D. Student, Department of Mechanical and Aerospace Engineering, University of Florida, Gainesville, Florida 32611-6250. Email: emilypalmer@ufl.edu.

<sup>&</sup>lt;sup>†</sup>Professor, Department of Mechanical and Aerospace Engineering, University of Florida, Gainesville, FL 32611-6250. E-mail: anilvrao@ufl.edu. Fellow AAS and Associate Fellow AIAA. Corresponding Author.

by the work of Ref. [1] where it was first formulated for unconstrained optimal control problems. In DOC, the uncertain parameters of interest are elevated to the level of states and the optimal control problem is augmented by a sensitivity matrix. The sensitivity matrix captures the sensitivity of the state at any time, t with respect to changes in the initial states, however the chain rule is applied to acquire the sensitivity of the state at the terminal time,  $t_f$ , with respect to changes in the state at arbitrary time, t. The sensitivity matrix then can be used to augment the optimal control problem, whether it be an additional term in the objective functional or a boundary condition. This methodology was then extended to constrained optimal control problems [2], and then even applied to a Mars Entry problem [3]. One issue with DOC is that the augmented optimal control problem t more complex than the original, as the number of states increases quadratically as a function of the number of original states and uncertain parameters. The increased dimensionality however can be decreased with the use of traditional uncertainty functions, with the trade-off of not being able to account for time-varying parametric uncertainties [4].

While desensitized optimal control has been shown to reduce the sensitivity of trajectories to uncertainty and disturbances, the resulting trajectory suffers from a loss of performance overall as a result. Ideally, the offline reference trajectory would be optimal, with the guidance updates being made such that the adjustments to uncertainty are performed in a way that is optimal from the point of where the guidance update is being implemented. Current guidance methods include proportional navigation (PN) [5, 6], linear-quadratic (LQ) methods [7, 8, 9], acceleration guidance [10], and neighboring optimal control (NOC) [11]. These methods however do not incorporate optimization and do not take into account the full non-linear dynamics of the vehicle, leading to loss of performance. In order to maximize performance when performing guidance updates, a methodology was developed that re-solved the optimal control problem in real time [12]. At each guidance update, the optimal control problem was re-solved with the original objective and boundary conditions using the current state as the new initial condition. The newly solved control was then simulated over the span of the guidance cycle period for the "real" vehicle, which was modeled with slight difference than the reference model in order to simulate uncertainties. The processes of re-solving the optimal control problem and simulating flight was repeated until the remaining horizon was shorter than the guidance cycle period. One issue with this methodology however was path constraint violations. The guidance framework did not explicitly account for path constraints, which lead to the "real" vehicle violating the constraints despite the solution obtained by solving the optimal control problem not revealing violations. In order to prevent violations, the guidance methodology was adjusted to explicitly deal with path constraints. Path constraints were explicitly accounted for by implementing contingency operations if the vehicle was approaching its physical limits and met a certain user-chosen percentage of its limits. The contingency operation guidance followed the previous methods steps, except for within the user-chosen range of a constraint limit, at which point the objective functional used to re-solve the optimal control problem was altered. The contingency objective functional maximized the margin between the constrained quantity and its limit. The guidance method was then applied to a Mars entry problem where the modeled surface level atmospheric density varied from the "real" flight atmospheric density. The problem was solved for two scenarios; one of which assumed there was a set error in the atmospheric density model, and one case where the error was made to be random at each guidance cycle. The random case was only explored for a singular simulation, therefore the results were not sufficient in proving the effectiveness of the method. This paper aims to further explore the case of random errors in the atmospheric model. A Monte Carlo simulation was performed to evaluate the effectiveness of the novel optimal guidance with contingencies method, and the results are presented in this paper.

#### BOLZA OPTIMAL CONTROL PROBLEM

Without loss of generality, consider the following optimal control problem in Bolza form. Determine the state,  $\mathbf{x}(\tau) \in \mathbb{R}^{n_x}$ , and the control,  $\mathbf{u}(\tau) \in \mathbb{R}^{n_u}$ , on  $\tau \in [-1, +1]$  that minimize the objective functional

$$J = \mathcal{M}(\mathbf{x}(-1), t_0, \mathbf{x}(+1), t_f) + \frac{t_f - t_0}{2} \int_{-1}^{+1} \mathcal{L}(\mathbf{x}(\tau), \mathbf{u}(\tau), t(\tau; t_0, t_f)) d\tau$$
 (1)

subject to the dynamic constraints

$$\frac{d\mathbf{x}}{d\tau} - \frac{t_f - t_0}{2} \mathbf{f}(\mathbf{x}(\tau), \mathbf{u}(\tau), t(\tau; t_0, t_f)) = \mathbf{0},\tag{2}$$

the inequality path constraints

$$\mathbf{c}_{\min} \le \mathbf{c}(\mathbf{x}(\tau), \mathbf{u}(\tau), t(\tau; t_0, t_f)) \le \mathbf{c}_{\max},$$
 (3)

and the boundary conditions

$$\mathbf{b}_{\min} \le \mathbf{b}(\mathbf{x}(-1), t_0, \mathbf{x}(+1), t_f) \le \mathbf{b}_{\max}. \tag{4}$$

It is noted that domain  $t \in [t_0, t_f]$  and the domain  $\tau \in [-1, +1]$  are related via the affine transformation

$$t(\tau; t_0, t_f) = \frac{t_f - t_0}{2} \tau + \frac{t_f + t_0}{2} \tag{5}$$

# LEGENDRE-GAUSS-RADAU COLLOCATION

Consider now the following partition of the Bolza optimal control problem described in Eqs. (1)–(4) into K mesh intervals. First, let  $(T_0,\ldots,T_K)\in[-1,+1]$  be such that  $T_0< T_1<\cdots< T_K$ . Furthermore, let  $T_0=-1$  and  $T_K=+1$ . Finally, let  $\mathcal{S}_k=[T_{k-1},T_k]$ . Next, let  $\mathbf{x}^{(k)}(\tau)$  and  $\mathbf{u}^{(k)}(\tau)$  be the state and control, respectively, in mesh interval  $\mathcal{S}_k$ . The Bolza optimal control problem given in Eqs. (1)–(4) is then formulated as a K mesh interval problem as follows. Minimize the objective functional:

$$J = \mathcal{M}(\mathbf{x}^{(1)}(-1), t_0, \mathbf{x}^{(K)}(+1), t_f) + \frac{t_f - t_0}{2} \sum_{k=1}^K \int_{T_{k-1}}^{T_k} \mathcal{L}(\mathbf{x}^{(k)}(\tau), \mathbf{u}^{(k)}(\tau), t(\tau; t_0, t_f)) d\tau,$$
(6)

subject to the dynamic constraints:

$$\frac{d\mathbf{x}^{(k)}}{d\tau} - \frac{t_f - t_0}{2} \mathbf{f}(\mathbf{x}^{(k)}(\tau), \mathbf{u}^{(k)}(\tau), t(\tau; t_0, t_f)) = \mathbf{0} \quad (k = 1, ..., K)$$
 (7)

the inequality path constraints:

$$\mathbf{c}_{\min} \le \mathbf{c}(\mathbf{x}^{(k)}(\tau), \mathbf{u}^{(k)}(\tau), t(\tau; t_0, t_f)) \le \mathbf{c}_{\max} \quad (k = 1, ..., K)$$
(8)

and the boundary conditions

$$\mathbf{b}_{\min} \le \mathbf{b}(\mathbf{x}^{(1)}(-1), t_0, \mathbf{x}^{(K)}(+1), t_f) \le \mathbf{b}_{\max}.$$
 (9)

It is noted that, in order to maintain continuity at each interior mesh point, the condition  $\mathbf{x}(T_k^-) = \mathbf{x}(T_k^+)$  (k=1,...,K-1) is enforced.

The partitioned optimal control problerm given in Eqs. (6)–(9) is discretized using Legendre-Gauss-Radau (LGR) collocation as described in Refs. [13, 14, 15, 16]. In the LGR method, the state in every mesh interval is approximated as

$$\mathbf{x}^{(k)}(\tau) \approx \mathbf{X}^{(k)}(\tau) = \sum_{j=1}^{N_k+1} \mathbf{X}_j^{(k)} \ell_j^{(k)}(\tau)$$
 (10)

where  $\ell_i^{(k)}(\tau)$  is the basis of Lagrange polynomials

$$\ell_j^{(k)}(\tau) = \prod_{i=1, i \neq j}^{N_k+1} \frac{\tau - \tau_i^{(k)}}{\tau_j^{(k)} - \tau_i^{(k)}}$$
(11)

and  $(\tau_1^{(k)},...,\tau_{N_k}^{(k)})$  are the LGR points in mesh interval  $\mathcal{S}_k$  and  $\tau_{N_k+1}^{(k)}=T_k$  is a noncollocated point. The derivative of the state approximation  $\mathbf{X}^{(k)}(\tau)$  is given as

$$\frac{d\mathbf{X}^{(k)}}{d\tau} = \sum_{j=1}^{N_k+1} \mathbf{X}_j^{(k)} \frac{d\ell_j^{(k)}}{d\tau}$$
 (12)

The dynamic constraints given by Eq. (7) are collocated at the  $N_k$  LGR points in mesh interval  $k \in [1,...,K]$  as

$$\sum_{j=1}^{N_k+1} D_{ij}^{(k)} \mathbf{X}_j^{(k)} - \frac{t_f - t_0}{2} \mathbf{f}(\mathbf{X}_i^{(k)}, \mathbf{U}_i^{(k)}, t_i^{(k)}) = \mathbf{0} \quad (i = 1, ..., N_k)$$
(13)

where  $t_i^{(k)} = t(\tau_i^{(k)}; t_0, t_f)$  and

$$D_{ij}^{(k)} = \left[\frac{d\ell_j^{(k)}}{d\tau}\right]_{\tau=\tau_i}, \ (i=1,\dots,N_K; j=1,\dots,N_{K+1})$$
(14)

are the elements of the  $N_k \times (N_k + 1)$  Legendre-Gauss-Radau differentiation matrix [13] in mesh interval  $S_k$ ,  $k \in [1, ..., K]$ . The LGR approximation then leads to the following nonlinear programming problem (NLP). Minimize

$$\mathcal{J} = \mathcal{M}(\mathbf{X}_{1}^{(1)}, t_{0}, \mathbf{X}_{N_{K}+1}^{(K)}, t_{f}) + \sum_{k=1}^{K} \sum_{i=1}^{N_{k}} \frac{t_{f} - t_{0}}{2} w_{j}^{(k)} \mathcal{L}(\mathbf{X}_{i}^{(k)}, \mathbf{U}_{i}^{(k)}, t_{i}^{(k)})$$
(15)

subject to the collocation constraints of Eq. (13), the discretized path constraints

$$\mathbf{c}_{\min} \le \mathbf{c}(\mathbf{X}_{i}^{(k)}, \mathbf{U}_{i}^{(k)}, t_{i}^{(k)}) \le \mathbf{c}_{\max} \quad (i = 1, ..., N_{k}),$$
 (16)

the discretized boundary conditions

$$\mathbf{b}_{\min} \le \mathbf{b}(\mathbf{X}_{1}^{(1)}, t_0, \mathbf{X}_{N_K+1}^{(K)}, t_f) \le \mathbf{b}_{\max},$$
 (17)

and the continuity constraints

$$\mathbf{X}_{N_k+1}^{(k)} = \mathbf{X}_1^{(k+1)}, \quad (k = 1, ..., K-1).$$
 (18)

#### OPTIMAL GUIDANCE WITH CONTINGENCY OPERATIONS

This section describes the methodology used when implementing guidance updates with contingency operations. The guidance updates described in this section were performed using LGR collocation on a shrinking horizon. The methodology explored in this paper is a modification and extension of the work presented in Refs. [17, 12]. In the previous work, the original optimal control problem was re-solved at the beginning of each guidance cycle,  $t_0 + k\Delta T$ , (where k is the guidance cycle number and  $\Delta T$  is the guidance cycle period) using the state at the current time as the initial condition. Then the control generated from the optimal solution was used to simulate the flight of the "real" vehicle over the guidance cycle period, and the process of re-solving the optimal control problem is repeated until the remaining horizon is shorter than the guidance cycle period. Originally, the guidance strategy did not explicitly account for path constraints during the "real" flight of the vehicle and it was found that when performing this method on the Mars entry problem, the path constraints were violated during flight. In order to address the issue of constraint violation, a modification was added to the method to explicitly deal with constraints.

The modified method can be summarized as follows. At the end of each guidance cycle period the values of the constrained quantities are evaluated and the current state is taken to be the initial condition for when re-solving the optimal control problem. In the Mars entry problem only upper constraints are considered, however generalizing, contingencies must be made for the four following cases: (1)  $c_{\rm max} > 0$ ; (2)  $c_{\rm max} < 0$ ; (3)  $c_{\rm min} > 0$ ; (4)  $c_{\rm min} < 0$ . In the event of case (1), the percentage of the total allowable constraint is computed and then used to determine the proximity the current constrained quantities are to their limit. This is computed as follows:

$$P(t) = \frac{c(\mathbf{x}(t), \mathbf{u}(t), t)}{c_{\text{max}}} \quad t \in [t_0 + k\Delta T, t_0 + (k+1)\Delta T], \tag{19}$$

where c is the scalar constraint quantity of interest and k is the current guidance cycle. The maximum value of P(t) is then compared to a user-chosen threshold,  $\alpha$ . The rate of change of the path constraint is also computed. If it is determined that the maximum percentage is larger than the user-chosen threshold and the constraint is increasing towards its limits, i.e.:

$$\max P(t) \ge \alpha \tag{20}$$

and

$$\dot{c} > 0 \tag{21}$$

then the contingency plan is activated. The following action is taken; when re-solving the optimal control problem, the objective functional used is changed from the reference objective to a new objective,  $J_2$ . The purpose of the new objective functional is to maximize the margin between the current path and its limit, therefore for the case of a positive upper constaint, the new objective will be a smooth approximation of the maximum value of the constraint function. For this study, the following smooth approximation was used as the objective functional:

$$J_2 = \min \frac{1}{\beta} \log \int_{t_0}^{t_f} \left( \exp(\beta \frac{c(t)}{c_{\text{max}}}) \right)$$
 (22)

where  $\beta$  is a user chosen parameter that can be adjusted in the mission planning phase in order to maximize performance of the guidance updates.

When the conditions given by Eq. (20) - (21) are not met, the original objective functional is used when re-solving the optimal control problem.

# PROBLEM FORMULATION

The Mars entry vehicle was modeled as a point mass over a spherical nonrotating planet, and the equations of motion were formulated as[18]:

$$\dot{r} = v \sin \gamma, 
\dot{v} = -D - g \sin \gamma, 
\dot{\theta} = \frac{v \cos \gamma \sin \psi}{r \cos \phi}, 
\dot{\phi} = \frac{v \cos \gamma \cos \psi}{r}, 
\dot{\gamma} = \frac{1}{v} \left[ L \cos \sigma + \left( \frac{v}{r} - \frac{g}{v} \right) \cos \gamma \right], 
\dot{\psi} = \frac{L \sin \sigma}{v \cos \gamma} + \frac{v \cos \gamma \sin \psi \tan \theta}{r},$$
(23)

where r is the vehicles radial distance from the center of the planet, v is the vehicles speed,  $\theta$  is the vehicles latitude,  $\phi$  being the vehicles longitude,  $\gamma$  is the flight path angle, and  $\psi$  is the vehicles heading angle, and  $g = \mu/r^2$ . The lift and drag specific forces were calculated as:

$$L = \frac{qC_LS}{m},$$

$$D = \frac{qC_DS}{m},$$
(24)

where  $C_L$  is the vehicles coefficient of lift,  $C_D$  is the vehicles coefficient of drag, S is the characteristic length, m is the vehicle mass (assumed to be constant),  $q = \rho v^2/2$  is the dynamic pressure,  $\rho = \rho_0 \exp(-h/H)$  is the atmospheric density, where, h = r - R is the altitude. The constants  $\rho_0$ , H, and R are the Martian sea level density, the density scale height, and the radius of the planet, respectively.

Physical constraints were placed on the vehicles dynamic pressure, sensed acceleration, and heating rate, given by the following equations:

$$q = \rho v^2 / 2 \le q_{\text{max}}, \tag{25}$$

$$A = \sqrt{L^2 + D^2} \le A_{\text{max}}, \tag{26}$$

$$q = \rho v^2 / 2 \leq q_{\text{max}},$$

$$A = \sqrt{L^2 + D^2} \leq A_{\text{max}},$$

$$\dot{Q} = K_q \left(\frac{\rho}{r_n}\right)^N v^M \leq \dot{Q}_{\text{max}},$$

$$(25)$$

$$\dot{Q} = K_q \left(\frac{\rho}{r_n}\right)^N v^M \leq \dot{Q}_{\text{max}},$$

$$(27)$$

where N, M, and  $K_q$  are constants, and  $g_0$  is the Earth sea level acceleration due to gravity.

The numerical values of the physical constants used in this paper are given in 1. The initial state and time were fixed, the final state was free with the exception of the terminal speed, and the values are given in Table 2. Additionally the limits on the state and path constraints are given by Table 3.

Table 1. Physical constants.

Quantity	Value	Quantity	Value
R	$3.386\times10^6~\mathrm{m}$	$r_n$	0.6 m
$\mu$	$4.284 \times 10^{13} \text{ m}^3/\text{s}^2$	M	3
$g_0$	$9.80665 \text{ m/}s^2$	N	0.5
S	$15.9~\mathrm{m}^2$	$K_q$	$1.9027 \times 10^{-8} \text{ W/cm}^2$
$C_D$	1.45	H	$9354~\mathrm{m}$
$C_L$	0.348	$\rho_0$	$0.0158~\mathrm{kg/m^3}$
m	$3300~\mathrm{kg}$		

The reference objective was to maximize the altitude at which the terminal speed was reach, or minimize

$$\min J_1 = -r(t_f). \tag{28}$$

Table 2. Boundary conditions.

Quantity	Value	Quantity	Value	
$r_0$	$3.5112 \times 10^6 \text{ m}$	$\theta_0$	0 rad	
$v_0$	6000 m/s	$\phi_0$	-0.0873 rad	
$\gamma_0$	-0.2007  rad	$\psi_0$	1.6581 rad	
$v_f$	540 m/s			

# SOLUTION OF THE OPTIMAL CONTROL PROBLEM

The optimal solutions presented in this paper were generated using the optimal control software  $\mathbb{GPOPS} - \mathbb{II}$ , which is an hp adaptive Gaussian quadrature collocation solver[13, 14, 15, 19, 20, 21, 22, 23]. The hp method has the benefit of allowing smaller meshes to be utilized than standard h methods, while still achieving the desired accuracy tolerances. In the hp method, mesh points are concentrated in areas where the solution is nonsmooth and rapidly changing, and places fewer mesh points in areas where the solution is smooth. The smoothness of the solution was approximated by determining the decay rate of the Legendre polynomial coefficients as a function of the coefficient index[23].  $\mathbb{GPOPS} - \mathbb{II}$  interfaces with the nonlinear programming problem solver, IPOPT, which is an interior point method. IPOPT was employed in full Newton mode and the first and second derivatives were determined using sparce central finite differencing.  $\mathbb{GPOPS} - \mathbb{II}$  supplies IPOPT with the objective function, Lagrangian Hessian, constraint Jacobian, boundary conditions, and dynamic constraint function. An initial guess and mesh are required inputs to  $\mathbb{GPOPS} - \mathbb{II}$ , and the solution/mesh from the previous guidance cycle was used as the initial guess when re-solving the optimal control problem.  $\mathbb{GPOPS} - \mathbb{II}$  then outputs the optimal solution, containing the control matrix and state matrix. It should be noted that while the results in this paper were obtained using  $\mathbb{GPOPS} - \mathbb{II}$ , any collocation method could be used with the outlined guidance strategy.

Table 3. Bounds on variables and constraints.

Quantity	Value	Quantity	Value	
$r_{ m min}$	$3.3862\times10^6~\mathrm{m}$	$r_{ m max}$	$3.5112\times10^6~\mathrm{m}$	
$v_{ m min}$	0.1 m/s	$v_{ m max}$	6000 m/s	
$ heta_{ m min}$	$-2\pi$ rad	$\theta_{ m max}$	$2\pi$ rad	
$\phi_{ m min}$	-1.2217  rad	$\phi_{ m max}$	1.2217 rad	
$\gamma_{ m min}$	-1.0472  rad	$\gamma_{ m max}$	0 rad	
$\psi_{ m min}$	$-2\pi$ rad	$\psi_{\mathrm{max}}$	$2\pi$ rad	
$\sigma_{ m min}$	0.05236 rad	$\sigma_{ m max}$	2.0944 rad	
$q_{\mathrm{min}}$	0 Pa	$q_{\rm max}$	10000 Pa	
$A_{\min}$	$0 \text{ m/s}^2$	$A_{\max}$	$5g_0 \text{ m/s}^2$	
$Q_{\min}$	0 W/cm <sup>2</sup>	$Q_{\max}$	70 W/cm <sup>2</sup>	

#### MONTE-CARLO ANALYSIS

This section describes the process used to evaluate the effectiveness of the newly outlined guidance strategy against random errors in the model used to solve the reference solution. The modeling error was simulated by using a reference model when solving the optimal control problem and simulating the flight of the "real" vehicle with a perturbed model. The only difference between the reference model and the perturbed model was the density model used, which are given as:

$$\rho_{ref} = \rho_0 \exp(-h/H), \tag{29}$$

$$\rho_{pert} = \tilde{\rho}_0 \exp(-h/H), \tag{30}$$

respectively, where  $\rho_0$  and  $\tilde{\rho}_0$  are the reference and perturbed surface level densities, h is the altitude, and H is the density scale height. In order to simulate random perturbations, the value of the surface level density,  $\tilde{\rho}_0$ , was drawn from a uniform distribution on  $[\rho_0, 1.05\rho_0]$  at the beginning of each guidance cycle. In order to analyze the effectiveness of the guidance algorithm for the guidance algorithm was run from entry to end of mission N times. For each N run of the guidance simulation, the following quantities were recorded: final state, final time, maximum values of each path constraint, and number of objective functional changes.

The result of the Monte Carlo simulation is a data set of N for the final state, final time, maximum path constraint values, and number of objective functional switches. The data then can be statistically analyzed to gather information on the effectiveness of the guidance algorithm at preventing path constraint violation, as well as give insight into performance loss due to the disturbances, i.e. lowered final altitude. The error between the final states for each sample in the Monte Carlo analysis will be computed with regards t the reference solution, that is the errors are defined as:

$$\delta_{\mathbf{x}} = \tilde{\mathbf{x}}(t_f) - \mathbf{x}(t_f) \tag{31}$$

where  $\tilde{\mathbf{x}}(t_f)$  is the final state of each sample and  $\mathbf{x}(t_f)$  is the final state of the reference solution. Additionally, the Monte Carlo simulations were used to choose the constant parameter,  $\beta$ , used in the contingency objective functional given by Eq. (22).

#### **RESULTS**

A Monte Carlo simulation was performed using N = 500 samples. Simulations were run using values of  $\beta=3,4$  for the constant parameter in the contingency objective functional. A value of  $\alpha=0.8$  was used to determine when to switch to contingency operations. A Monte Carlo analysis was was also completed for the guidance strategy without contingency operations. For each simulation, guidance updates were performed every 10 seconds. The results of the simulations are presented in this section and compared to the reference solution.

#### **Reference Solution**

The optimal control problem was solved using the reference model. The final state of the vehicle was determined to be:

$$x = [3396634 \text{ m}, 540 \text{ m/s}, 0.306 \text{ rad}, -0.137 \text{ rad}, -0.246 \text{ rad}, 2.07 \text{ rad}]$$
 (32)

The speed versus altitude was plotted, as well as the control (Fig. 1).

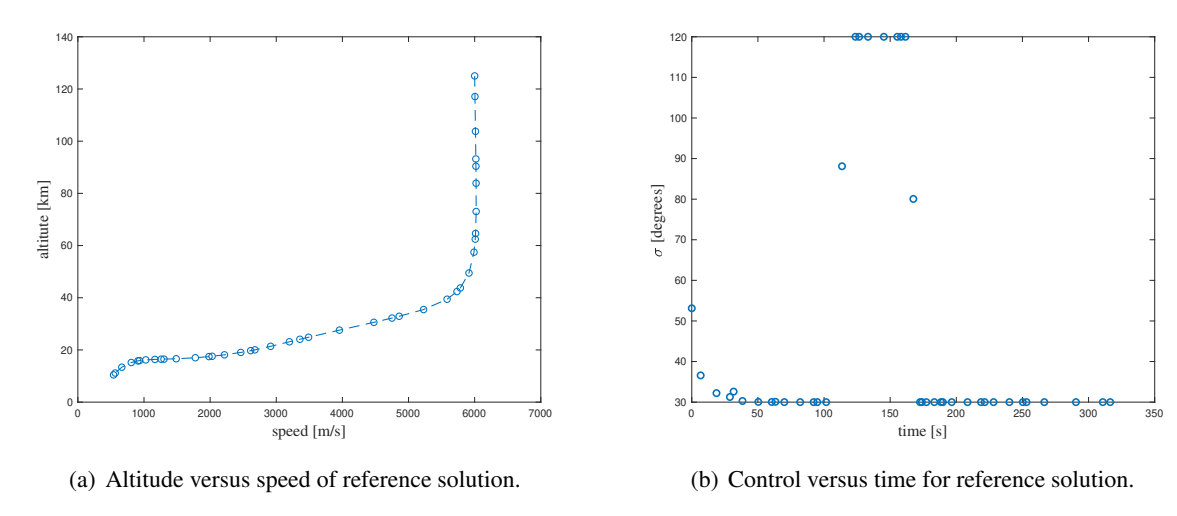


Figure 1. Reference Solution.

# **Results without Contingency Operation**

The following results represent the guidance algorithm being employed without contingency operations. Out of the N=500 Monte Carlo simulations performed, the acceleration load path constraint was violated for 475 runs, the heat rate constraint was violated for 40 runs, and the dynamic pressure constraint was kept under the limit. Figure 2 depicts the error in the final states at each sample of the Monte Carlo analysis. Figure 3 shows the maximum path constraint values at each sample. The results illustrate the need to explicitly account for path constraints when executing guidance updates, as even small perturbations away from the reference solution can lead to constraint violation. Additionally, the altitude versus speed, and control was plotted for a single run (Fig. 4).

Table 4. Results for guidance scheme without contingency operations

Measure	$h(t_f)$	$v(t_f)$	$t_f$	$\max A$	$\max \dot{Q}$	$\max q$
Mean Value	10.67 km	539.9 m/s	310.6 s	$5.08 g_0$	69.53 W/cm <sup>2</sup>	6.94 KPa
Standard Deviation	52.6 m	0.2147 m/s	0.352 s	$0.050 g_0$	$0.337 \text{ W/cm}^2$	67.5 Pa
Highest Value	10. 81 km	540 m/s	311.5 s	$5.21 g_0$	70.28 W/cm <sup>2</sup>	7.11 KPa
Lowest Value	10. 50 km	538 m/s	309.9 s	$4.94 g_0$	68.5 W/cm <sup>2</sup>	6.74 KPa

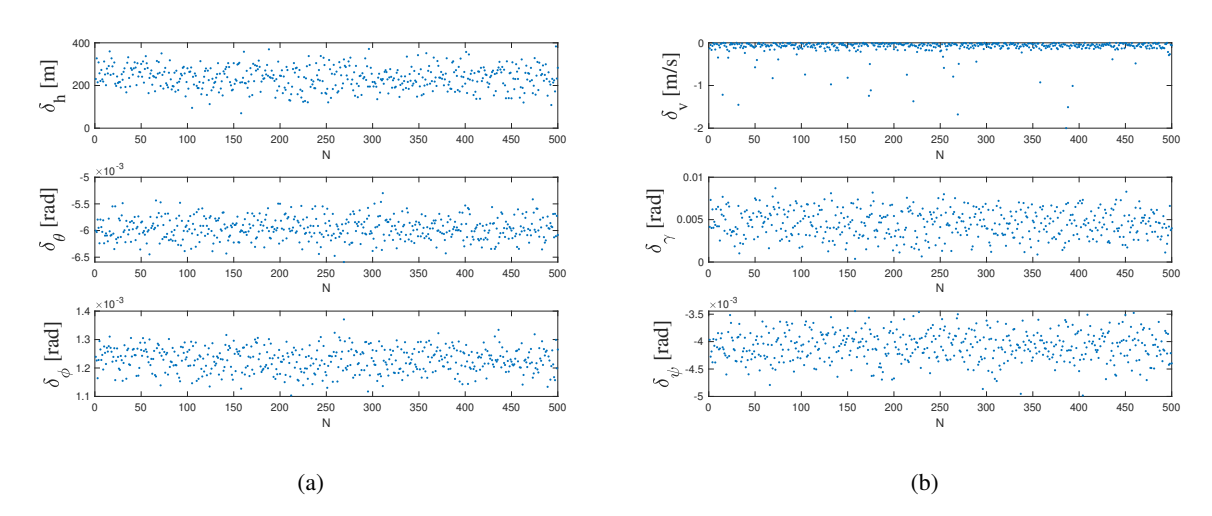


Figure 2. Error of final states at each sample without contingency operations.

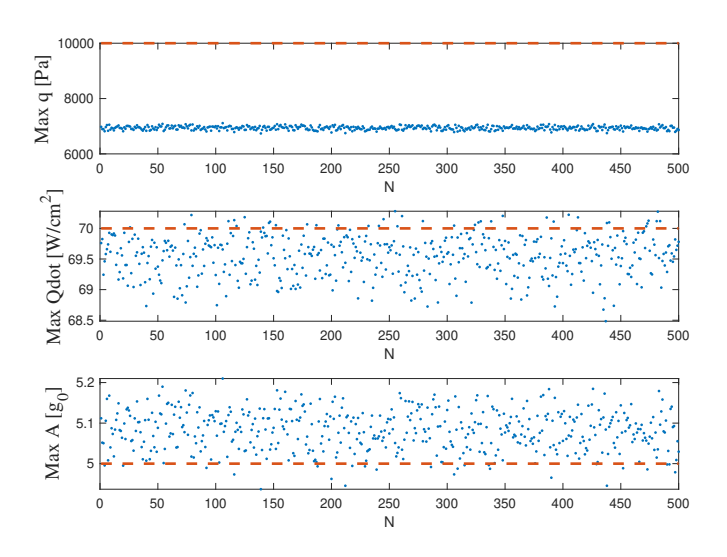
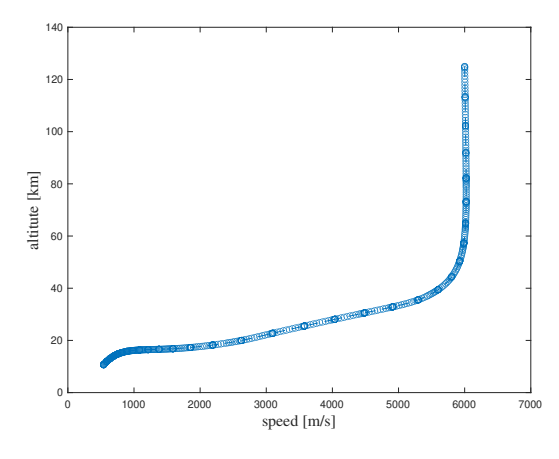
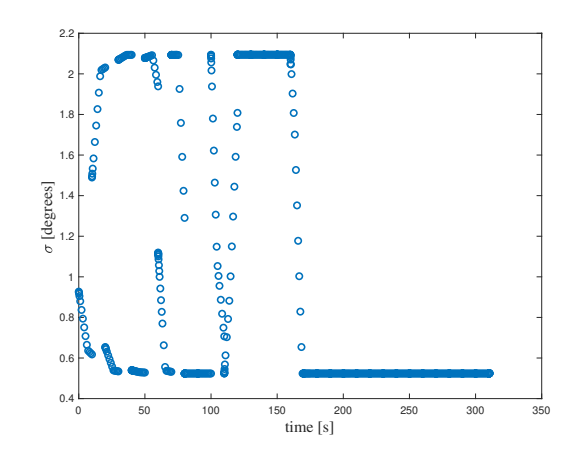


Figure 3. The maximum value of each constrained quantity for each sample without contingency operations. The dashed line represents the true limit of the vehicle.





(a) Altitude versus speed for a single run.

(b) Control versus time for a single run.

Figure 4. Results for a single sample of the guidance scheme employed without contingency operations.

# **Results for** $\beta = 3$

The guidance algorithm was run for N=500 samples using  $\beta=3$ . The tabulated results are given in Table 5. The guidance algorithm was able to successfully prevented path constraint violations for each simulation. The error in the final state with regards to the reference solution was plotted for each sample (Fig. 5), as well as the maximum path constraint values (Fig. 6). Additionally, the control and state was plotted for a single sample (Fig. 7).

 $\max Q$ Measure  $h(t_f)$  $v(t_f)$  $\max A$  $t_f$  $\max q$ 68.9 W/cm<sup>2</sup> Mean Value 10.21 km 539.22 m/s 325.9 s  $4.83 g_0$ 6.59 KPa Standard Deviation  $0.050 g_0$ 0.353 W/cm<sup>2</sup> 62.83 m 0.4402 m/s 1.24 s 67.5 Pa 69.94 W/cm<sup>2</sup>  $4.94 g_0$ Highest Value 540 m/s 6.74 KPa 10. 50 km 327.4 s 10. 07 km 67.96 W/cm<sup>2</sup> Lowest Value 538.2 m/s 316.15 s  $4.71 g_0$ 6.42 KPa

Table 5. Results for  $\beta = 3$ 

# Results for $\beta = 4$

The guidance algorithm was run for N=500 samples using  $\beta=4$ . The tabulated results are given in Table 6. The guidance algorithm was able to successfully prevented path constraint violations for each simulation. The error in the final state with regards to the reference solution was plotted for each sample (Fig. 8), as well as the maximum path constraint values (Fig. 9). Additionally, the control and state was plotted for a single sample (Fig. 10).

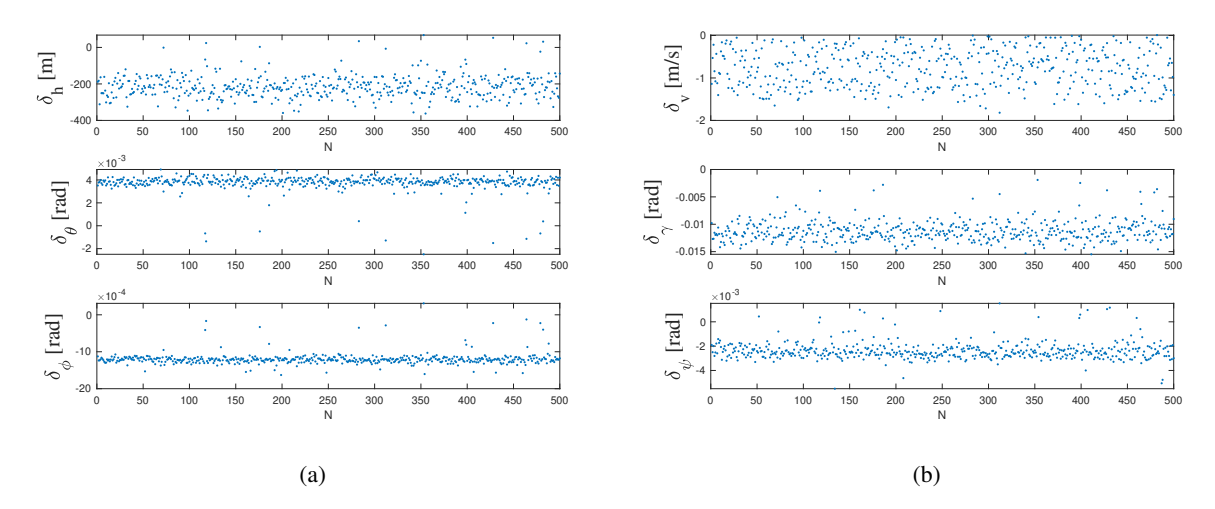


Figure 5. Error of final states at each sample using a value of  $\beta = 3$ .

Table 6. Results for  $\beta = 4$ 

Measure	$h(t_f)$	$v(t_f)$	$t_f$	$\max A$	$\max \dot{Q}$	$\max q$
Mean Value	10.22 km	539.21 m/s	326.2 s	$4.82 g_0$	68.9 W/cm <sup>2</sup>	6.58 KPa
Standard Deviation	54.92 m	0.4423 m/s	0.523 s	$0.0495 g_0$	$0.343 \text{ W/cm}^2$	64.93 Pa
Highest Value	10. 37 km	540 m/s	328.09 s	$4.94 g_0$	69.66 W/cm <sup>2</sup>	6.74 KPa
Lowest Value	10. 04 km	538.3 m/s	321.3 s	$4.69 g_0$	67.95 W/cm <sup>2</sup>	6.41 KPa

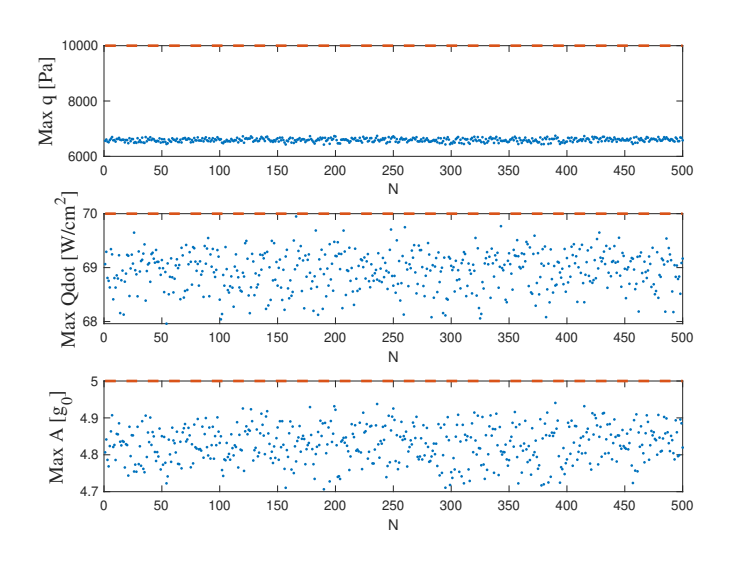


Figure 6. The maximum value of each constrained quantity for each sample using a value of  $\beta=3$ . The dashed line represents the true limit of the vehicle.

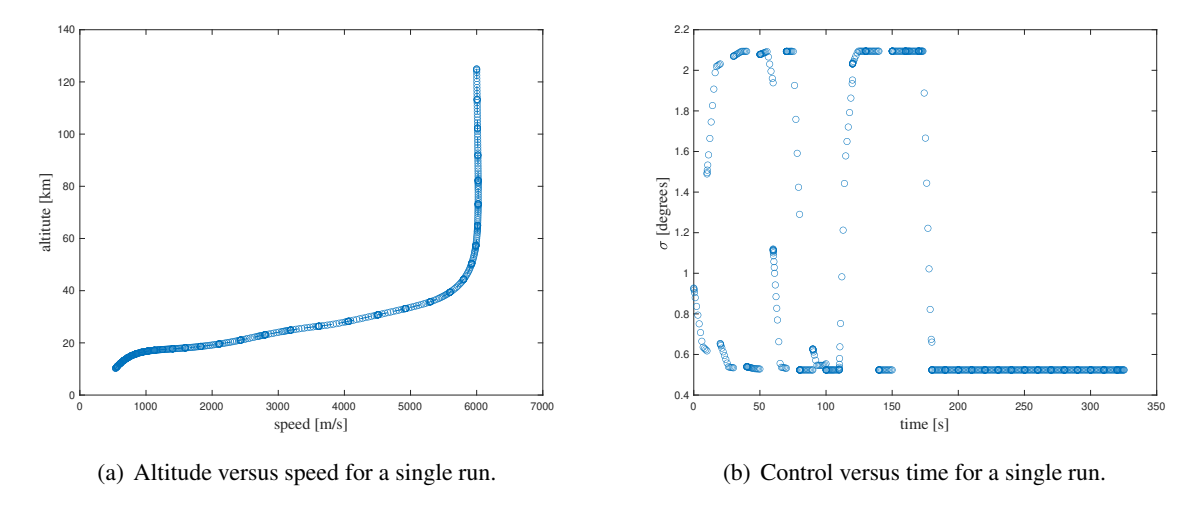


Figure 7. Results for a single sample using a value of  $\beta=3$ .

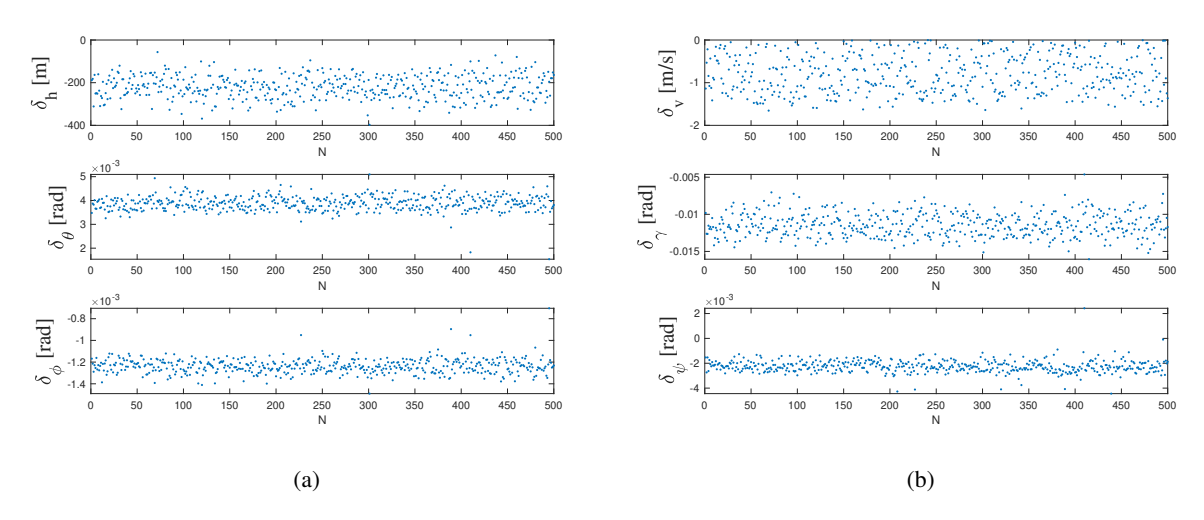


Figure 8. Error of final states at each sample using a value of  $\beta=4$ .

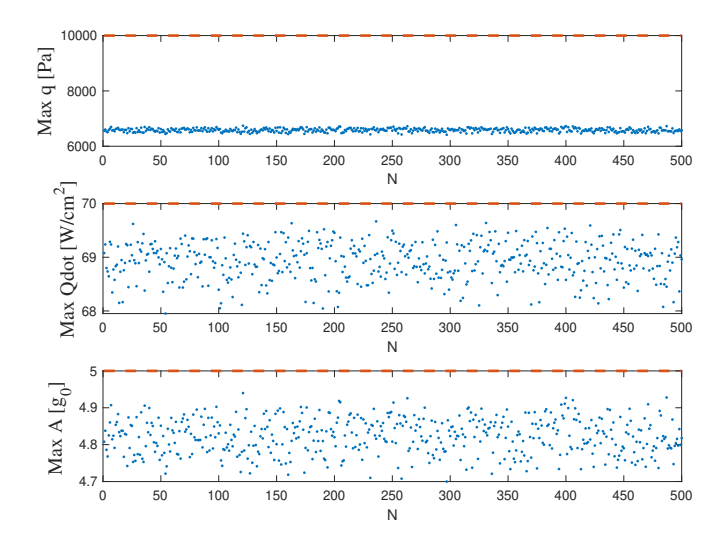


Figure 9. The maximum value of each constrained quantity for each sample using a value of  $\beta=4$ . The dashed line represents the true limit of the vehicle.

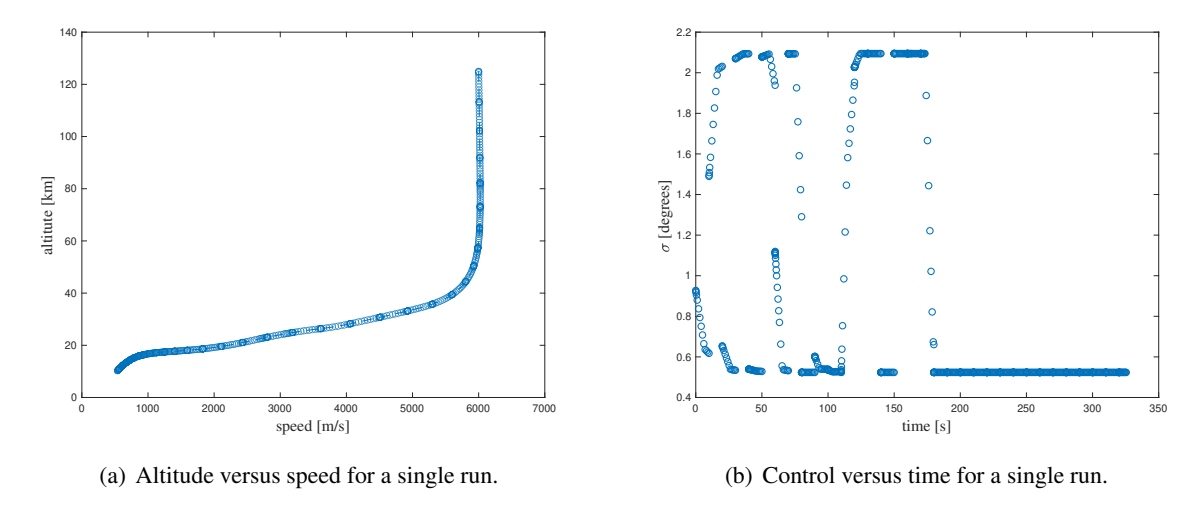


Figure 10. Results for a single sample using a value of  $\beta=4$ .

# **CONCLUSION**

An optimal guidance scheme employing contingency operations to prevent path constraint violations was presented. The guidance scheme was applied to a Mars entry problem where it was assumed that there was a modeling error in the surface level atmospheric density. Monte Carlo analyses were performed to evaluate the effectiveness of the guidance scheme and was compared to the reference trajectory. Additionally, the guidance scheme was employed without contingency operations. The surface level atmospheric density was drawn from a uniform distribution on  $[\rho_0, 1.05\rho_0]$  at the beginning of each guidance cycle to simulate perturbations. It was found that without contingency operations, the heating rate constraint was violated for 95 % of the Monte Carlo simulations. Employing contingency operations, the path constraint violations were eliminated completely. These results indicate that the proposed guidance scheme with contingency operations has merit and should be further explored for path constrained flight.

#### ACKNOWLEDGMENTS

The authors gratefully acknowledge support for this research from the U.S. National Science Foundation under grant CMMI-2031213 and from the U.S. Air Force Research Laboratory under contract FA8651-21-F-1041.

# REFERENCES

- [1] H. Seywald and R. Kumar, "Desensitized optimal trajectories," Vol. 93, jan 1996, pp. 103–113.
- [2] K. Seywald and H. Seywald, "Desensitized Optimal Control," *AIAA Scitech 2019 Forum*, American Institute of Aeronautics and Astronautics, jan 2019, 10.2514/6.2019-0651.
- [3] S. Li and Y. Peng, "Mars entry trajectory optimization using DOC and DCNLP," *Advances in Space Research*, Vol. 47, Feb. 2011, pp. 440–452, 10.1016/j.asr.2010.09.005.
- [4] V. Makkapati, M. Dor, et al., "Trajectory Desensitization in Optimal Control Problems," 2018 IEEE Conference on Decision and Control (CDC), Institute of Electrical and Electronics Engineers (IEEE), dec 2018, 10.1109/CDC.2018.8619577.
- [5] P. Zarchan, *Tactical and Strategic Missile Guidance*, Vol. 239. Reston, VA: Progress in Astronautics and Aeronautics, AIAA, 6 ed., 2012.
- [6] X. Liu, Z. Shen, and P. Lu, "Closed-Loop Optimization of Guidance Gain for Constrained Impact," Journal of Guidance, Control, and Dynamics, Vol. 40, February 2017, pp. 453–460. https://doi. org/10.2514/1.G000323.
- [7] M. Kim and K. V. Grider, "Terminal Guidance for Impact Attitude Angle Constrained Flight Trajectories," *IEEE Transactions on Aerospace and Electronic Systems*, Vol. AES-9, November 1973, pp. 852–859. https://doi.org/10.1109/TAES.1973.309659, 10.1109/TAES.1973.309659.
- [8] A. Farooq and D. J. N. Limebeer, "Optimal Trajectory Regulation for Radar Imaging Guidance," *Journal of Guidance, Control, and Dynamics*, Vol. 31, July–August 2008, pp. 1076–1092. https://doi.org/10.2514/1.31441.
- [9] V. Shaferman and T. Shima, "Linear Quadratic Guidance Laws for Imposing a Terminal Intercept Angle," *Journal of Guidance, Control, and Dynamics*, Vol. 31, September–October 2008, pp. 1400–1412. https://doi.org/10.2514/1.32836.
- [10] J. C. Harpold and C. A. Graves, "Shuttle Entry Guidance," *Journal of the Astronautical Sciences*, Vol. 27, No. 3, 1981, pp. 239–268.
- [11] M. R. Jardin and A. E. B. Jr., "Neighboring Optimal Aircraft Guidance in Winds," *Journal of Guidance, Control, and Dynamics*, Vol. 24, July–August 2001, pp. 710–715. https://doi.org/10.2514/2.4798.
- [12] E. M. Palmer and A. V.Rao, "Mars Entry Optimal Trajectory Generation, Guidance, and Control," AIAA Scitech 2022 Forum, American Institute of Aeronautics and Astronautics, jan 2022, 10.2514/6.2022-2390.
- [13] D. Garg, M. A. Patterson, W. W. Hager, A. V. Rao, D. A. Benson, and G. T. Huntington, "A Unified Framework for the Numerical Solution of Optimal Control Problems Using Pseudospectral Methods," *Automatica*, Vol. 46, November 2010, pp. 1843–1851. DOI: 10.1016/j.automatica.2010.06.048.

- [14] D. Garg, W. W. Hager, and A. V. Rao, "Pseudospectral Methods for Solving Infinite-Horizon Optimal Control Problems," *Automatica*, Vol. 47, April 2011, pp. 829–837. DOI: 10.1016/j.automatica.2011.01.085.
- [15] D. Garg, M. A. Patterson, C. L. Darby, C. Francolin, G. T. Huntington, W. W. Hager, and A. V. Rao, "Direct Trajectory Optimization and Costate Estimation of Finite-Horizon and Infinite-Horizon Optimal Control Problems via a Radau Pseudospectral Method," *Computational Optimization and Applications*, Vol. 49, June 2011, pp. 335–358. DOI: 10.1007/s10589–00–09291–0.
- [16] M. A. Patterson, W. W. Hager, and A. V. Rao, "A ph mesh refinement method for optimal control," *Optimal Control Applications and Methods*, Vol. 36, July–August 2015, pp. 398–421, 10.1002/oca.2114.
- [17] M. E. Dennis, W. W. Hager, and A. V. Rao, "Computational Method for Optimal Guidance and Control Using Adaptive Gaussian Quadrature Collocation," *Journal of Guidance, Control, and Dynamics*, Vol. 42, Sept. 2019, pp. 2026–2041, 10.2514/1.G003943.
- [18] J. T. Betts, Practical Methods for Optimal Control and Estimation Using Nonlinear Programming. SIAM, 2010.
- [19] C. L. Darby, W. W. Hager, and A. V. Rao, "An hp-Adaptive Pseudospectral method for Solving Optimal Control Problems," *Optimal Control Applications and Methods*, Vol. 32, Aug. 2010, pp. 476–502, 10.1002/oca.957.
- [20] C. L. Darby, D. Garg, and A. V. Rao, "Costate Estimation using Multiple-Interval Pseudospectral Methods," *Journal of Spacecraft and Rockets*, Vol. 48, Sept. 2011, pp. 856–866, 10.2514/1.a32040.
- [21] M. A. Patterson and A. V. Rao, "GPOPS-II," ACM Transactions on Mathematical Software, Vol. 41, oct 2014, pp. 1–37, 10.1145/2558904.
- [22] F. Liu, W. W. Hager, and A. V. Rao, "Adaptive mesh refinement method for optimal control using nonsmoothness detection and mesh size reduction," *Journal of the Franklin Institute*, Vol. 352, oct 2015, pp. 4081–4106, 10.1016/j.jfranklin.2015.05.028.
- [23] F. Liu, W. W. Hager, and A. V. Rao, "Adaptive Mesh Refinement Method for Optimal Control Using Decay Rates of Legendre Polynomial Coefficients," *IEEE Transactions on Control Systems Technology*, Vol. 26, July 2018, pp. 1475–1483, 10.1109/tcst.2017.2702122.